ACS APPLIED MATERIALS & INTERFACES

Research Article

www.acsami.org

Light-Induced Efficient Molecular Oxygen Activation on a Cu(II)-Grafted TiO_2/Graphene Photocatalyst for Phenol Degradation

Hui Zhang, Liang-Hong Guo,* Dabin Wang, Lixia Zhao, and Bin Wan

State Key Laboratory of Environmental Chemistry and Eco-toxicology, Research Centre for Eco-environmental Sciences, Chinese Academy of Sciences, 18 Shuangqing Road, P.O. Box 2871, Beijing 100085, China

Supporting Information

ABSTRACT: An efficient photocatalytic process involves two closely related steps: charge separation and the subsequent surface redox reaction. Herein, a ternary hybrid photocatalytic system was designed and fabricated by anchoring Cu(II) clusters onto a TiO_2/reduced graphene oxide (RGO) composite. Microscopic and spectroscopic characterization revealed that both TiO_2 nanoparticles and Cu(II) clusters were highly dispersed on a graphene sheet with intimate interfacial contact. Compared with pristine TiO_2, the TiO_2/RGO/Cu(II) composite yielded an almost 3-fold enhancement in the photodegradation rate toward phenol degradation under UV irradiation. Electron spin resonance (ESR) spectra and electrochemical measurements demonstrated that the improved photocatalytic activity of this ternary system benefitted from the synergetic effect between RGO and Cu(II), which facilitates the interfacial charge transfer and simultaneously achieves in situ generation of H_2O_2 via two-electron reduction of O_2. These results highlight the importance to harmonize the charge separation and surface reaction process in achieving high photocatalytic efficiency for practical application.

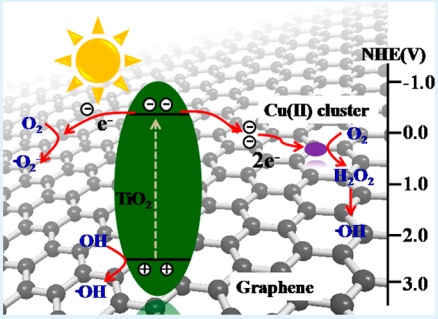

KEYWORDS: *TiO_2, photocatalysis, oxygen reduction, phenol degradation*

INTRODUCTION

Photoinduced oxidation/reduction reactions at the semiconductor surface present a promising approach to address the emerging environmental issues.[1−3] In a typical photocatalytic reaction, molecular oxygen is activated by photogenerated electrons to produce $\bullet O_2^-$ or H_2O_2, while holes are trapped by surface-absorbed hydroxyls (OH^-) to generate $\bullet OH$.[4] These reactive oxygen species (ROS) are identified as one of the most active initiators of photocatalytic degradation of organic contaminants. Previous studies demonstrate that the photocatalytic efficiency is critically dependent upon light adsorption, electron/hole separation, and surface chemical reactions.[5] Unfortunately, optimizing all these processes in a single photocatalyst has remained a great challenge. Although UV-light-excited wide-band-gap photocatalysts (e.g., TiO_2) usually exhibit more efficiency in initiating or accelerating photodegradation reaction because of the high redox potential of the photogenerated electron/hole in the conduction/valence band,[6] the quantum efficiency of molecular oxygen activation is often hindered due to the charge recombination in photoexcited semiconductors and the lack of active sites on the catalyst surface.

To overcome these problems, heterostructured photocatalysts have been constructed to improve the quantum efficiency of TiO_2.[7,8] For example, TiO_2/carbon nanomaterial (e.g., C_{60}, carbon nanotube) hybrids greatly promoted the charge separation across their interface.[9,10] Metal nanoparticles (e.g., Au, Ag, and Pt) were used to quickly capture electrons from photoexcited TiO_2.[11,12] In recent years, to avoid the high cost of noble-metal nanoparticles, surface modification of TiO_2 with transition metal ions (such as Cu(II) and Fe(III)) has been employed to promote the multielectron reduction reaction of oxygen and subsequently enhance the photocatalytic performance.[13−17] However, the increased quantum efficiency of Cu(II)- or Fe(III)-grafted TiO_2 is still limited due to the weak charge separation ability in the hybrid system. Indeed, both charge separation and surface catalytic reaction are equally important, and the slower one will be the rate-determining step for the photocatalytic reaction. The challenge in achieving a high-performance photocatalyst lies in ensuring a harmony of charge separation and the subsequent surface catalytic reaction for molecular oxygen activation, which requires deliberate control of the interactions among the photocatalyst components in a systematic and rational fashion.

With its monolayer structure and superior electron mobility, graphene is highly desirable as a flexible two-dimensional (2D) catalyst support.[18−20] Recently, graphene-based photocatalysts have been demonstrated to manipulate the charge transfer across the semiconductor−graphene interface.[21,22] Upon excitation of TiO_2 by light, electrons are transferred into RGO, which then participate in red-/ox- reaction or lead to their storage within the C−C network in the absence of an additional electron acceptor.[23,24] These elaborate works provide a hint to interface the light-harvesting semiconductor and

Received: October 28, 2014
Accepted: January 3, 2015
Published: January 3, 2015

DOI: 10.1021/am507483q
ACS Appl. Mater. Interfaces 2015, 7, 1816−1823

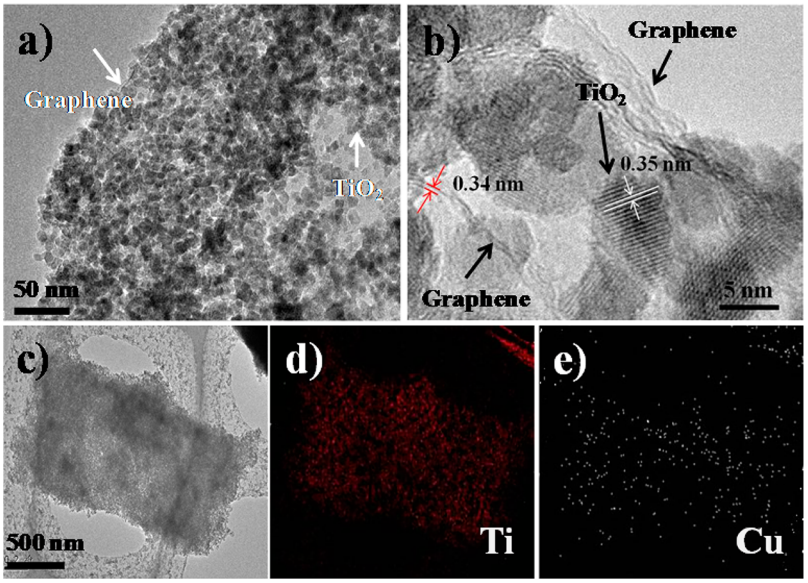

Figure 1. (a) TEM and (b) high-resolution TEM image of the prepared TiO_2/RGO/Cu(II) composite. (c–e) EDX element mapping images of Ti and Cu in the TiO_2/RGO/Cu(II) composites.

surface reaction sites onto an individual RGO sheet to accelerate the charge transfer process and surface catalytic reaction simultaneously. Herein, we report for the first time anchoring Cu(II) on a TiO_2/RGO mat to achieve an efficient photocatalytic process for phenol degradation. The charge transfer and molecular oxygen activation process in the system were investigated to explore the possible reaction mechanism. Our work demonstrates a promising way to simultaneously tune charge separation and molecular oxygen activation and consequently the overall photocatalytic performance.

EXPERIMENTAL SECTION

Chemicals and Materials. Graphite powder was purchased from Bodi Chemical Co. Ltd. (Tianjin, China). $Ti(OCH_4)_4$, phenol, and 5,5-dimethyl-1-pyrroline-*N*-oxide (DMPO) were purchased from Sigma-Aldrich (St. Louis, MO, USA). HPLC-grade methanol was obtained from Fisher Scientific (Pittsburgh, PA, USA). All other chemicals were of analytical grade and used as received. All solutions were prepared with deionized (DI) water obtained using a Millipore Milli-Q water purification system (Bedford, MA, USA).

Synthesis of Photocatalysts. Graphene oxide (GO) was synthesized by oxidation–exfoliation of graphite powder according to a modified Hummers' method.[25] TiO_2/RGO composites were prepared by a hydrothermal method. Typically, GO (3.3 mg) was dispersed in a mixed solution containing ethanol (15 mL) and water (30 mL) by ultrasonic treatment. Then, a solution of $Ti(OC_4H_9)_4$ (2.9 mL) and ethanol (15 mL) was added dropwise to the GO suspension under magnetic stirring. After stirring for 2 h, a homogeneous suspension with a light gray color was obtained and then transferred into a 100 mL Teflon-lined autoclave and maintained at 180 °C for 10 h. The resultant TiO_2/RGO composite was collected by centrifugation, washed repeatedly by water and ethanol, and dried under vacuum at room temperature. A blank TiO_2 sample was prepared following a similar method without the addition of GO.

The grafting of Cu(II) ions onto TiO_2/RGO composites was performed using an impregnation method. In a typical preparation, the TiO_2/RGO sample (0.5 g) was dispersed into $CuCl_2$ solution (20 mL). The weight fraction of Cu^{2+} ions relative to TiO_2/RGO was set to be 1%. Then, the suspension was heated at 90 °C for 1 h using a water bath under stirring. The resultant suspension was collected by centrifugation, washed by distilled water, and dried at 90 °C for 24 h. The final products were ground into a powder using an agate mortar. The TiO_2/Cu(II) sample was prepared following the same method.

Characterizations. The morphology of the synthesized photocatalysts was investigated by transmission electron microscopy (TEM) using a JEOL JEM 2010 instrument (Tokyo, Japan) operated at 120 kV. The elemental mapping images were acquired using a scanning TEM attachment by equipping with an Oxford energy-dispersive X-ray detector (EDX) (Bucks, U.K.). For TEM measurements, a droplet of the sample ethanol solution was put onto a Mo grid. Structural characterization of the prepared samples was performed by powder X-ray diffraction (XRD) on an X'Pert Pro MPD (Eindhoven, Netherlands) with Cu Kα radiation (λ = 0.15418 nm) and Raman spectra on a Renishaw InVia Raman spectrometer (Wotton-under-Edge, U.K.) with exciting wavelength at 532 nm. The ionic characteristics were investigated by X-ray photoelectron spectroscopy (XPS) on a Thermo VG ESCALAB 250 spectrometer (East Grinsted, UK) with Al Kα radiation at 1486.6 eV. Elemental analyses of the samples were performed using an inductively coupled plasma/optical emission spectrometer (ICP-OES) on a PerkinElmer Optima 8300 model instrument (Norwalk, CT, USA). Brunauer–Emmett–Teller (BET) surface area was obtained at 77 K on a QuadraSorb SI analyzer (Quantachrome, USA). Fluorescence spectra were measured on a Horiba Fluoromax-4 spectrofluorimeter (Edison, NJ, USA). The electron spin resonance (ESR) signal of the paramagnetic radicals trapped by 5,5-dimethyl-1-pyrroline-*N*-oxide (DMPO) was recorded on a Bruker ER073 spectrometer (Karlsruhe, Germany) during irradiation of the suspension (catalyst samples, 0.05 mg/mL; DMPO, 100 mM) with a 500 W mercury lamp. The settings were the following: center field 3503.95 G, microwave frequency 9.84 GHz, and power 20 mW. Electrochemical experiments were performed in a three-electrode cell on a CHI 630B workstation (Shanghai, China) with a platinum plate as the counter electrode and a saturated KCl Ag/AgCl electrode as the reference electrode. The working electrodes were prepared by coating photocatalyst–ethanol slurry onto FTO glass, and a small amount of Nafion solution (0.5%) was added to paste the slurry. Current–potential curves and cyclic voltammograms of the prepared electrode were measured in a 0.1 M $NaClO_4$ electrolyte solution. High-purity O_2 gas was used to bubble the electrolyte during the electrochemical O_2 reduction experiments. The normal hydrogen electrode (NHE) potential was converted from the Ag/AgCl electrode using $E_{NHE} = E_{(Ag/AgCl)} + 0.197$ V. Electrochemical impedance spectra (EIS) were measured in 0.1 M KCl solution containing 2.5 mM $K_3[Fe(CN)_6]/K_4[Fe(CN)_6]$ (1:1) by applying 5

DOI: 10.1021/am507483q
ACS Appl. Mater. Interfaces 2015, 7, 1816–1823

mV alternative signal versus the reference electrode over the frequency range of 1 MHz to 100 mHz.

Evaluation of Photocatalytic Properties. Photodegradation of a phenol solution in ambient condition was performed to evaluate the photocatalytic activity of the prepared catalysts. Typically, an aqueous solution containing phenol (50 mL, 10 mg/L) and a photocatalyst (50 mg) was placed in a cylindrical Pyrex glass vessel and kept in the dark for 30 min to ensure adsorption/desorption equilibrium. Then the photoreaction vessel was irradiated by a 500 W tubelike high-pressure mercury lamp with an irradiation intensity of 1.0 mW/cm^2 and the main emission wavelength at 365 nm. The suspension was continuously stirred by a Teflon-coated magnetic stirrer bar during the irradiation. The temperature of the reaction solution was maintained at 20 °C by recirculating a cooling water system during the reaction. At given time intervals, aliquots of the irradiated solution were collected, centrifuged, and analyzed by a high-performance liquid chromatograph (HPLC) on Aligent 1260 (Palo Alto, CA, USA) with a Poroshell 120 EC-C18 column. The mobile phase was methanol and water (v:v = 0.55:0.45) at a flow rate of 0.3 mL min^{-1}, and the detection wavelength was set at 280 nm.

H_2O_2 generation during UV irradiation of the photocatalyst solution was determined by dimerization of *p*-hydrophenylacetic acid (POPHA) in the presence of H_2O_2 and horseradish peroxidase to yield a fluorescence product 5,5′-dicarboxymethyl-2,2-dihydroxybiphenyl (λ_{ex} = 315 nm, λ_{em} = 406 nm).[26] Aliquots (0.5 mL) of irradiated catalyst solution were taken out and kept in the dark for 30 min. Subsequently, 0.5 mL of the fluorometric reagent (8 mg of POPHA and 2 mg of horseradish peroxidase dissolved in 50 mL of Tris buffer (0.1 M, pH 8.8) solution) was added and allowed to react for 30 min. Then, the above solution was centrifuged, and the supernatant was taken for fluorescence measurement. The calibration curves were obtained by standard additions of H_2O_2 to fluorometric reagents.

RESULTS AND DISCUSSION

Characterization of the TiO_2/RGO/Cu(II) Composite. A Cu(II)-grafted TiO_2/RGO composite was synthesized by a two-step process: (i) anchoring TiO_2 nanoparticles (NPs) on the RGO sheet as a 2-D scaffold and (ii) adsorption of Cu(II) on TiO_2/RGO. The AFM image shows GO exists as fragments with a thickness of ca. 1.1 nm (Figure S1 in the Supporting Information (SI)), which confirms the structure of a one- or few-layered GO sheet with oxygen-functional groups upon chemical exfoliation. These oxygen groups on the GO sheet would facilitate *in situ* growth of TiO_2 nanocrystals.[27] Meanwhile, the negative potential of GO given by these oxygen-functional groups could induce Cu^{2+} adsorption through electrostatic interactions.[28] Figure 1a shows typical TEM images of the resulting TiO_2/RGO/Cu(II) composites. It can be seen that spherically structured TiO_2 NPs are uniformly anchored on a 2-D RGO sheet with a crystallite size of ca. 8 nm (Figure S2, SI). Both TiO_2 NPs and the edge of the RGO sheet are evident. Such decorated TiO_2 NPs can act as a spacer to partially prevent the exfoliated graphene sheet from stacking. High-resolution TEM images (Figure 1b) exhibit a lattice fringe spacing of 0.35 nm, which can be assigned to anatase (101) planes of TiO_2, and a layered structure with interlayer spacing of 0.34 nm corresponding to RGO.[29] It needs to be noted that, compared with TiO_2/RGO hybrids (Figure S3, SI), surface modification with Cu(II) does not change their morphology and size in the ternary composite. Cu(II) on TiO_2/RGO samples is hardly observed by TEM, probably due to the limited amount of Cu(II) and an amorphous form at the low-grafting temperature.[13] However, EDX spectra confirm the presence of Cu(II). Figure 1c−e displays the representative element mapping images of Ti and Cu in the hybrids, demonstrating a homogeneous distribution of TiO_2 NPs and Cu(II) on the RGO sheet. Thus, an intimate interfacial contact among TiO_2, RGO, and Cu(II) components was achieved.

The structure character of the TiO_2/RGO/Cu(II) composites was further determined by XRD patterns (Figure S4, SI). TiO_2 in all the samples crystallizes in an anatase phase structure (JCPDS No. 21-1272). Notably, a characteristic (002) peak of GO at 2θ = 7.76° (corresponding to an interlayer distance of ~1.1 nm) disappeared completely after the hydrothermal process, suggesting the great reduction of GO and the successful intercalation of TiO_2 NPs and Cu(II) to the GO stacks in the final composites. No peaks associated with Cu-like compounds were detected, implying Cu(II) exists as an amorphous form. Raman spectra provide addition insights into the structure information on the composites (Figure 2).

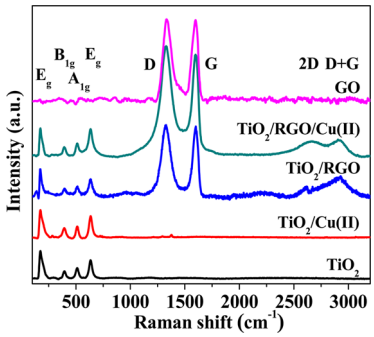

Figure 2. Raman spectra of GO, TiO_2, TiO_2/Cu(II), TiO_2/RGO, and TiO_2/RGO/Cu(II) composites.

The Raman bands at 144 cm^{-1} (E_g), 399 cm^{-1} (B_{1g}), 513 cm^{-1} (A_{1g}), and 638 cm^{-1} (E_g) match well with the TiO_2 anatase structure.[30] Two bands at 1326 cm^{-1} (D band) and 1597 cm^{-1} (G band) confirm the presence of RGO in the composites.[31] Significantly, a characteristic 2D band (at ~2665 cm^{-1}) corresponding to sp^2-bonded carbon atoms is also observed in the TiO_2/RGO/Cu(II) hybrid. It is noted that the intensity ratio (I_{2D}/I_G) usually reflects the recovery degree of sp^2-hybridized graphitic structure.[32] The increase of I_{2D}/I_G ratio to 0.14 after the solvothermal process demonstrates an efficient restoration of sp^2 carbon in GO. This would favor the formation of 2-D catalyst assembly with high quality.

Further evidence for the interactions of components in the TiO_2/RGO/Cu(II) composites comes from XPS spectra (Figure 3). A successful reduction of GO to RGO by the solvothermal process is verified by the C 1s signal, according to the diminished C−O, C═O, and O−C═O groups intensity. It is worth noting that the remaining C−O group but with much lower intensity (blue dashed line) in the composites provides the adsorption sites for Cu(II) anchoring. Moreover, a characteristic peak at 288.7 eV can be assigned to the Ti−O−C bond, suggesting that TiO_2 NPs interact with the RGO sheet through an esterification reaction.[27,30] The successful loading of Cu(II) on the TiO_2/RGO is further demonstrated by the Cu $2p_{3/2}$ core-level XPS signal at 923.6 eV, which is consistent with previous results.[13,14] By analogy with the reported Cu(II)−TiO_2 system, Cu(II) is grafted on the TiO_2/RGO composites in a distorted, amorphous CuO structure with a five-coordinated square pyramidal form. Although it is difficult to measure the location of Cu(II) in the composites, the Cu(II) cluster may prefer to attach on the RGO sheet due to the great complex ability of oxygen-containing groups

DOI: 10.1021/am507483q
ACS Appl. Mater. Interfaces 2015, 7, 1816−1823

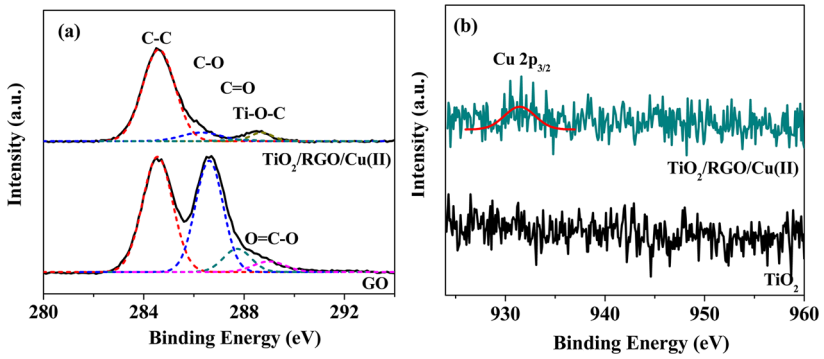

Figure 3. (a) Deconvoluted peaks of C 1s spectra of GO and TiO_2/RGO/Cu(II) samples. (b) Cu 2p core-level spectra of TiO_2 and TiO_2/RGO/Cu(II) samples.

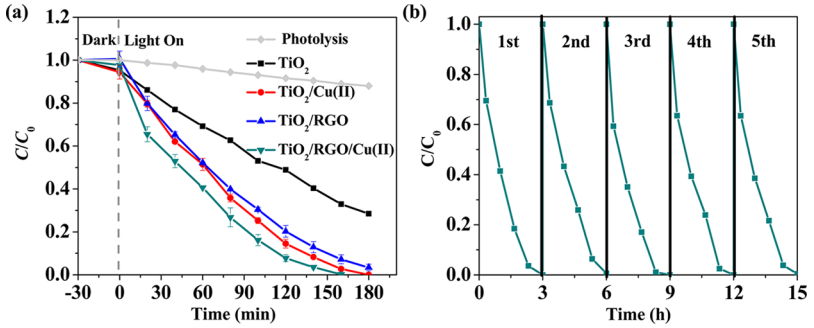

Figure 4. (a) Phenol degradation curves under UV light irradiation over TiO_2, TiO_2/Cu(II), TiO_2/RGO, and TiO_2/RGO/Cu(II) composites. (b) Cycling runs of TiO_2/RGO/Cu(II) for photocatalytic degradation of phenol.

toward Cu^{2+} ions. ICP-OES measurements displayed that the loading amount of Cu(II) was calculated to be ~0.92 wt % in the TiO_2/RGO/Cu(II) composites, nearly equal to the starting ratios used in the preparation. The cyclic voltammograms of the prepared TiO_2/RGO/Cu(II) electrode provide additional evidence for the loading of Cu(II) (Figure S5, SI). A couple of redox peaks were obviously observed, which are similar to the redox peaks of a Cu^{2+} solution on a bare TiO_2 electrode. The reduction peak located at about 0.10 V is assigned to the reduction of Cu(II) to Cu(I).[33] In the reverse scan, a major oxidation peak at 0.24 V is detected and attributed to Cu(I) oxidation. These results indicate that Cu(II) clusters are successfully grafted on TiO_2/RGO composites.

Photocatalytic Performance of the TiO_2/RGO/Cu(II) Catalyst. Phenol, a typical toxic aromatic compound with low degradability by the conventional decomposition method, was selected as the target molecule to evaluate the photocatalytic activity of the prepared composites. Figure 4a shows the phenol degradation curves over various photocatalysts under UV light irradiation. Both the direct photolysis of phenol and the adsorption of phenol on catalysts in the dark are negligible, suggesting the observed phenol degradation is initiated by semiconductor photocatalysis. Under UV light irradiation, the unmodified TiO_2 sample shows a low photocatalytic activity. It is evident that the introduction of RGO and Cu(II) resulted in a significant improvement in the photocatalytic phenol degradation. The temporal evolutions of phenol concentration are well fitted with a pseudo-first-order rate equation. The rate constants (k) for TiO_2/Cu(II), TiO_2/RGO, and TiO_2/RGO/Cu(II) composites are calculated to be 0.017, 0.014, and 0.023 min^{-1}, respectively, which is up to almost 3-fold enhancement compared to the bare TiO_2 (0.006 min^{-1}) (Figure S6, SI). Both TiO_2/Cu(II) and TiO_2/RGO exhibit a decent photocatalytic activity, which might arise from efficient molecular oxygen activation by Cu(II) clusters[17] and enhanced charge separation by RGO,[21,22] respectively. Importantly, the highest photocatalytic activity of TiO_2/RGO/Cu(II) clearly demonstrates Cu(II) and RGO act synergistically in boosting the photocatalytic performance of TiO_2.

A separate experiment of TiO_2/RGO/Cu(II) in the N_2-purged suspension under UV light shows a negligible phenol degradation, indicating that O_2 participates in the photocatalytic degradation reaction of organic pollutants. Once O_2 is consumed by photogenerated electrons for phenol degradation, it would be immediately supplied from air. Dissolved oxygen analysis displayed that its concentration was maintained at 8.50 mg/L during the photocatalysis process. Indeed, as the only molecule that can be reduced in ambient atmosphere, molecular O_2 activation during photocatalysis can not only inhibit the recombination of electron−hole pairs by capturing electrons but also yield $\bullet O_2^-$ or H_2O_2, which would participate in the subsequent photocatalytic reaction. To further investigate the improved photocatalytic performance of the TiO_2/RGO/Cu(II) composite, the generation of reactive oxygen species (ROS) during UV light irradiation was probed. A DMPO spin-trapping ESR technique was employed to detect $\bullet O_2^-$ and •OH generation (Figure S7, SI). No signal was observed under the dark. Upon UV light irradiation, a characteristic quartet peak of the DMPO−•OH adduct with intensity ratio of 1:2:2:1 was clearly observed. $\bullet O_2^-$ was also captured to form the DMPO−$\bullet O_2^-$ adduct with a quartet of peaks in methanol suspension, which usually is accompanied by the DMPO−$\cdot CH_2OH$ adduct signal due to the attack of •OH radicals onto the CH_3OH solvent molecules.[34] These results reveal that both $\bullet O_2^-$ and •OH were generated from the irradiated photocatalyst samples.

DOI: 10.1021/am507483q
ACS Appl. Mater. Interfaces 2015, 7, 1816−1823

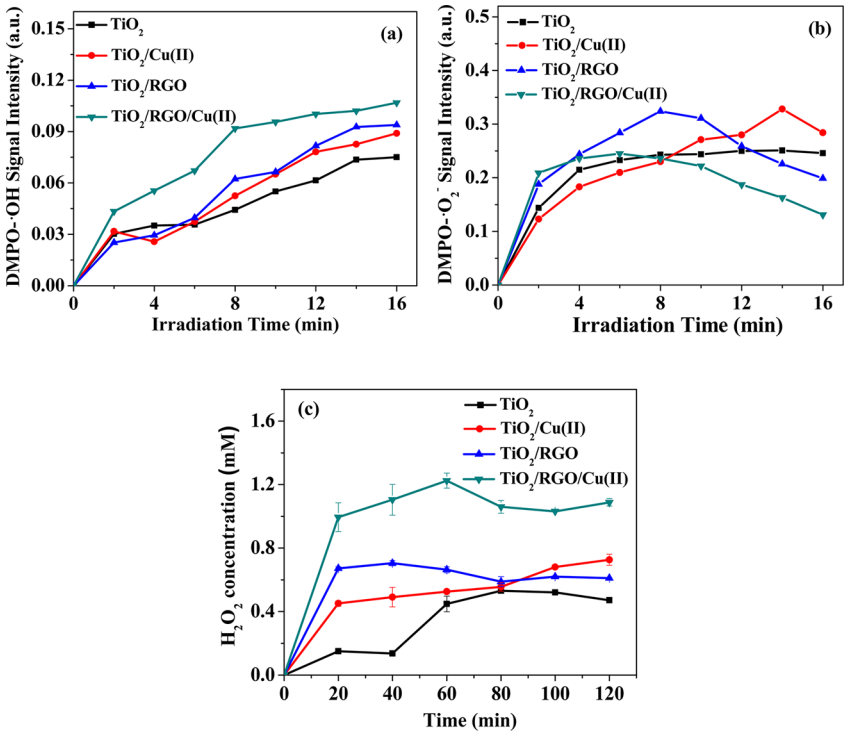

Figure 5. (a, b) Temporal evolution curves of the DMPO−•OH adduct and DMPO−•O_2- adduct obtained from the first peak intensity. (c) The generation curves of H_2O_2 over different samples under UV light irradiation.

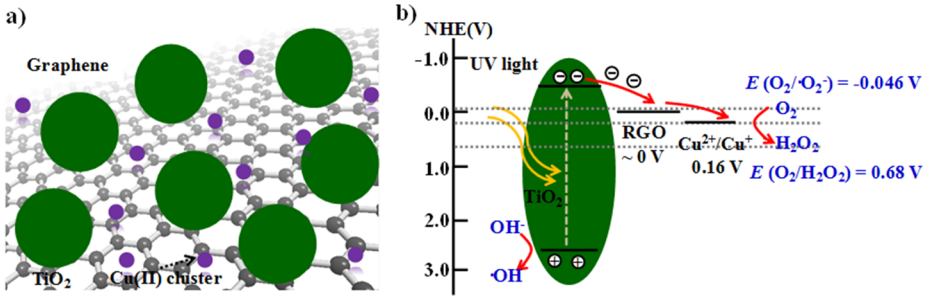

Figure 6. Schematic illustration of the structure of TiO_2/RGO/Cu(II) composites (a) and the possible photocatalytic process (b).

To further assess ROS generation, temporal evolutions of the ESR signal were displayed in Figure 5a and 5b, which were performed under the same conditions for comparison. It displays that the rate of •OH generation increases in the order of TiO_2/RGO/Cu(II) > TiO_2/RGO ≈ TiO_2/Cu(II) > TiO_2, the trend of which is in good agreement with the observed phenol degradation. In general, •OH radicals can generate from the photogenerated holes oxidation ($h^+ + OH^- = •OH$) O_2 reduction by electrons and/or both. Figure 5b displays that, after Cu(II) modification, the rate of •O_2- generation over TiO_2/RGO/Cu(II) is inhibited compared with that over TiO_2/RGO. Indeed, photogenerated electrons in the catalyst system could reduce O_2 to •O_2- or H_2O_2 via a one- or two-electron reduction process, respectively ($O_2 + e^- = •O_2$-, −0.046 V vs NHE; $O_2 + 2H^+ + 2e^- = H_2O_2$, 0.682 V vs NHE).[35] Thus, a POPHA fluorescence method was employed to determine H_2O_2 generation amount from different photocatalysts and further check the pathway of molecular oxygen activation (Figure 5c). It was found that significantly more H_2O_2 was generated over TiO_2/RGO/Cu(II) than TiO_2/RGO, which is contrary to the trend of •O_2- generation. The rapid formation of H_2O_2 and slow growth of •O_2- indicate that one two-electron reduction pathway ($O_2 \rightarrow H_2O_2$) is governed over TiO_2/RGO/Cu(II), while a one-electron reduction process for ·O_2- generation is the main pathway over TiO_2/RGO. Although the generated •O_2- can further convert into H_2O_2 by the subsequent reaction, the amount of generated H_2O_2 became steady after 40 min irradiation, indicating H_2O_2 was produced independent of •O_2-. This result further suggests that H_2O_2 is generated via a two-electron reduction of O_2 under the catalytic action of the grafted Cu(II) cluster. Indeed, considering the work function of RGO (−4.42 eV) and the Fermi level of RGO at about 0 V (vs NHE), which is lower than that of Cu^{2+}/Cu^+ (0.16 V vs NHE),[28,36] Cu^{2+} clusters could notably capture the accumulated electrons on the RGO sheet. In addition, the potential of Cu^{2+}/Cu^+ is more positive than the one-electron reduction of $O_2 \rightarrow$ •O_2-. Thus, a multielectron reduction pathway for H_2O_2 is more favored over TiO_2/RGO/Cu(II). This result is consistent with the multielectron reduction of O_2 over the reported Cu(II)/TiO_2, Fe(III)/TiO_2, and Rh(III)/TiO_2 system.[15,16,37] BET surface area analysis displayed that the introduction of RGO and Cu(II) did not alter the surface area of TiO_2 (Table S1, SI), indicating that the enhanced photoreactivity of the TiO_2/RGO/Cu(II) was not ascribed to

DOI: 10.1021/am507483q
ACS Appl. Mater. Interfaces 2015, 7, 1816−1823

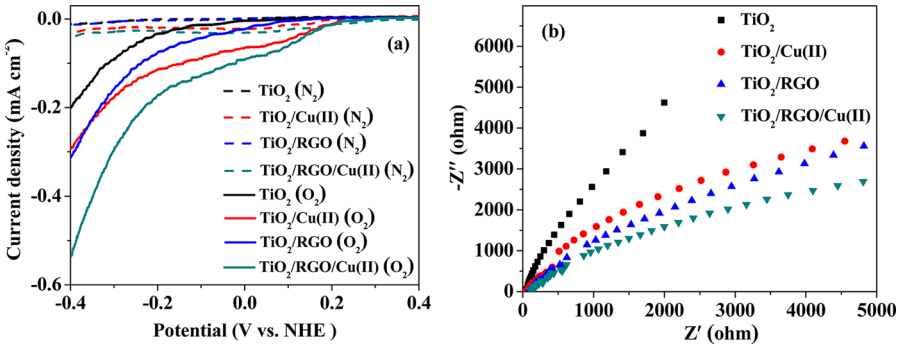

Figure 7. (a) Current−potential curves of the prepared electrodes in Ar- or O_2-saturated $NaClO_4$ solutions. (b) EIS Nyquist plots of the prepared electrodes in 0.1 M KCl solution containing 2.5 mM $K_3[Fe(CN)_6]/K_4[Fe(CN)_6]$ (1:1).

the difference of surface area. Thus, it can be concluded that the grafted Cu(II) clusters on TiO_2/RGO work as efficient reactive sites to transfer the photogenerated electrons to the O_2 molecule, resulting in a highly efficient multielectron reduction of O_2 to H_2O_2. The greatly enhanced ROS generation demonstrates the synergic effect of RGO and Cu(II) in promoting charge carrier separation.

On the basis of the above results, a schematic illustration of the photocatalytic reaction mechanism over TiO_2/RGO/Cu(II) is shown in Figure 6. RGO was demonstrated to store and shuttle electrons to the surface-adsorbed species.[23] Upon UV light irradiation, a stepwise transfer of electrons from photoexcited TiO_2 to the Cu(II) cluster via RGO (which acts as a "highway" for electron shuttling) occurs and subsequently achieves O_2 multielectron reduction. This process allows photogenerated holes and electrons to carry out selective catalytic reactions at separate sites. Owing to the efficient consumption of electrons, more remaining holes participate in the subsequent photocatalytic degradation reaction. Since the Cu^+/Cu^{2+} redox system provides only one electron, twice the amount of Cu species is required to achieve two-electron reduction of oxygen molecules ($O_2 + 2Cu^+ + 2H^+ = H_2O_2 + 2Cu^{2+}$). This structure has been confirmed by the aforementioned XPS results. The generated H_2O_2 could be further converted into •OH radicals through a Fenton-like reaction ($Cu^+ + H_2O_2 = Cu^{2+} + •OH + OH^-$)[28] or photocatalytic reactions (H_2O_2 + UV light = 2•OH and $H_2O_2 + e^- = •OH + OH^-$).[38] This indicates the synergetic effect between RGO and Cu(II) not only suppresses the charge recombination by improving the interfacial charge transfer but also facilitates the surface catalytic reaction by providing reactive centers. In addition, some photogenerated electrons can also be transferred directly to Cu(II) on the TiO_2 surface or to RGO and subsequently participate in photocatalytic reaction, which is consistent with the decent photocatalytic activity over TiO_2/Cu(II) and TiO_2/RGO composites.

The photocatalytic performance of the prepared composites under visible light irradiation (λ > 400 nm) was further investigated (Figure S8, SI). The bare TiO_2 showed rather poor photocatalytic activity under visible light, while TiO_2/Cu(II), TiO_2/RGO, and TiO_2/RGO/Cu(II) composites exhibited much improvements in the photocatalytic degradation of phenol. These results indicate the narrowing of the band gap of TiO_2 after Cu(II) and RGO incorporation, which can be attributed to the photoinduced interfacial charge transfer between TiO_2 and the adsorbed Cu(II) species[13,14,36] and the formation of the Ti−O−C band in the TiO_2/RGO composites,[39,40] respectively. However, the photocatalytic efficiency of these composites under visible light is still low.

To evaluate the stability of the TiO_2/RGO/Cu(II) photocatalyst, a recycling photocatalytic experiment was carried out. As shown in Figure 4b, the high performance of TiO_2/RGO/Cu(II) was well maintained during the repeated light irradiation cycles. Moreover, the amount of Cu(II) species in the five-cycle repeated TiO_2/RGO/Cu(II) was about 0.87 wt %, which is comparable to the as-prepared TiO_2/RGO/Cu(II) composites. Few Cu species in the photocatalytic reaction solution also indicated the good stability of Cu(II) in the composites (Figure S9, SI). Thus, the high photocatalytic activity and stability of TiO_2/RGO/Cu(II) composites suggest its great potential in practical applications.

Electrochemical Measurements of TiO_2/RGO/Cu(II) Catalyst. To further examine the oxygen reduction process, electrochemical O_2 reduction was investigated on the prepared catalyst film electrode at bias potential to avoid the complicated redox process under light irradiation conditions. Figure 7a shows the current−potential curves of the prepared composite electrodes in Ar- or O_2-saturated electrolyte. Little current was observed in Ar-bubbled solution regardless of the electrodes, while in O_2-saturated solution a reduction current was observed, indicating that O_2 reduction occurred on the composite electrodes. Compared with the bare TiO_2 electrode, a larger O_2 reduction current is observed over TiO_2/RGO and TiO_2/Cu(II) electrodes due to the important roles of RGO and Cu(II) in promoting charge transfer and facilitating O_2 reduction, respectively. Under the synergetic effect of RGO and Cu(II), the TiO_2/RGO/Cu(II) ternary system exhibited the highest O_2 reduction current. Another interesting observation is that the onset potential for oxygen reduction gradually shifted from below 0 V on TiO_2 and TiO_2/RGO electrode, which corresponds to one-electron reduction of O_2, to the positive region (about 0.15 V) in the case of the Cu(II)-grafted electrode, in good agreement with the redox potential of Cu^{2+}/Cu^+. At this potential, multielectron reduction of O_2 probably occurred for H_2O_2 generation. Thus, the electrochemical oxygen reduction behavior of the electrodes further demonstrates that the grafted Cu^{2+} accepts electrons from TiO_2 via RGO and then transfers electrons to O_2 via multielectron reduction reaction, which is consistent with the observed ROS generation during the photocatalysis process.

The charge-carrier migration behavior in the TiO_2/RGO/Cu(II) ternary system was further characterized by EIS spectra (Figure 7b). Compared with the pure TiO_2 sample, both TiO_2/Cu(II) and TiO_2/RGO show depressed semicircles at high frequencies, suggesting a decrease in the contact resistance at

DOI: 10.1021/am507483q
ACS Appl. Mater. Interfaces 2015, 7, 1816−1823

the solid-state interface layer and the charge transfer resistance at the electrode−electrolyte solution contact interface.[41] Notably, the TiO_2/RGO/Cu(II) ternary system exhibited the shortest circle among all three hybrid samples, indicating a faster interfacial charge transfer and more efficient charge separation due to the excellent electron shuttling feature of RGO and effective Cu(II) cluster reactive sites for electron capture. The efficient charge transport behavior was further confirmed by the cyclic voltammograms (Figure S4, SI). The anodic and cathodic current density of Cu(II) on the TiO_2/RGO/Cu(II) composite electrode is larger than that of TiO_2/Cu(II), implying enhanced electron transfer due to the introduction of the RGO sheet as a 2-D conducting substrate. These results demonstrate the significant role of RGO and Cu(II) in improving charge separation and subsequent O_2 activation for photocatalytic application.

CONCLUSION

In summary, the Cu(II)-grafted TiO_2/reduced graphene oxide (RGO) composite was prepared for developing a high-performance photocatalyst. Under the synergetic effect between RGO and Cu(II), this composition engineering not only optimizes charge transfer pathways for improved charge separation but also provides abundant photocatalytic reactive sites to reduce oxygen effectively, resulting in enhanced photocatalytic performance for phenol degradation. In addition, Cu(II) cluster modified TiO_2/RGO preferentially reduces O_2 to H_2O_2 via two-electron transfer. The modulation of charge separation and the molecule oxygen activation pathway described here can be potentially applied to other photocatalysis systems for environmental cleanup.

ASSOCIATED CONTENT

Supporting Information

AFM image of GO, size distribution of TiO_2 NPs in TiO_2/RGO/Cu(II) composites, TEM images of TiO_2/RGO, XRD patterns, cyclic voltammograms, ESR spectra of OH and $\bullet O_2^-$ species, BET surface area and visible light photoactivity of the prepared photocatalysts, and Cu-species concentration in the TiO_2/RGO/Cu(II) composite suspension. This material is available free of charge via the Internet at http://pubs.acs.org.

AUTHOR INFORMATION

Corresponding Author

*Phone: 86 10-62849685. E-mail: lhguo@rcees.ac.cn.

Notes

The authors declare no competing financial interest.

ACKNOWLEDGMENTS

This work was supported by the National Basic Research Program of China (2011CB936001) and National Nature Science Foundation of China (21207146, 21177138, and 21477146).

REFERENCES

(1) Hoffmann, M. R.; Martin, S. T.; Choi, W.; Bahnemann, D. W. Environmental Applications of Semiconductor Photocatalysis. *Chem. Rev.* **1995**, *95*, 69−96.

(2) Tachikawa, T.; Fujitsuka, M.; Majima, T. Mechanistic Insight into the TiO_2 Photocatalytic Reactions: Design of New Photocatalysts. *J. Phys. Chem. C* **2007**, *111*, 5259−5275.

(3) Teoh, W. Y.; Scott, J. A.; Amal, R. Progress in Heterogeneous Photocatalysis: from Classical Radical Chemistry to Engineering Nanomaterials and Solar Reactors. *J. Phys. Chem. Lett.* **2012**, *3*, 629−639.

(4) Xu, W.; Jain, P. K.; Beberwyck, B. J.; Alivisatos, A. P. Probing Redox Photocatalysis of Trapped Electrons and Holes on Single Sb-doped Titania Nanorod Surfaces. *J. Am. Chem. Soc.* **2012**, *134*, 3946−3949.

(5) Tong, H.; Ouyang, S.; Bi, Y.; Umezawa, N.; Oshikiri, M.; Ye, J. Nano-photocatalytic Materials: Possibilities and Challenges. *Adv. Mater.* **2012**, *24*, 229−251.

(6) Liu, M.; Qiu, X. Q.; Miyauchi, M.; Hashimoto, K. Energy-Level Matching of Fe(III) Ions Grafted at Surface and Doped in Bulk for Efficient Visible-Light Photocatalysts. *J. Am. Chem. Soc.* **2013**, *135*, 10064−10072.

(7) Kubacka, A.; Fernández-García, M.; Colón, G. Advanced Nanoarchitectures for Solar Photocatalytic Applications. *Chem. Rev.* **2012**, *112*, 1555−1614.

(8) Yang, J.; Wang, D.; Han, H.; Li, C. Roles of Cocatalysts in Photocatalysis and Photoelectrocatalysis. *Acc. Chem. Res.* **2013**, *46*, 1900−1909.

(9) Lin, J.; Zong, R.; Zhou, M.; Zhu, Y. Photoelectric Catalytic Degradation of Methylene Blue by C_{60}-modified TiO_2 Nanotube Array. *Appl. Catal., B* **2009**, *89*, 425−431.

(10) Kongkanand, A.; Kamat, P. V. Electron Storage in Single Wall Carbon Nanotubes. Fermi Level Equilibration in Semiconductor−SWCNT Suspensions. *ACS Nano* **2007**, *1*, 13−21.

(11) Wang, F.; Jiang, Y.; Gautam, A.; Li, Y.; Amal, R. Exploring the Origin of Enhanced Activity and Reaction Pathway for Photocatalytic H_2 Production on Au/B-TiO_2 Catalysts. *ACS Catal.* **2014**, *4*, 1451−1457.

(12) Su, R.; Tiruvalam, R.; He, Q.; Dimitratos, N.; Kesavan, L.; Hammond, C.; Lopez-Sanchez, J. A.; Bechstein, R.; Kiely, C. J.; Hutchings, G. J.; Besenbacher, F. Promotion of Phenol Photodecomposition over TiO_2 Using Au, Pd, and Au-Pd Nanoparticles. *ACS Nano* **2012**, *6*, 6284−6292.

(13) Irie, H.; Miura, S.; Kamiya, K.; Hashimoto, K. Efficient Visible Light-sensitive Photocatalysts: Grafting Cu(II) Ions onto TiO_2 and WO_3 Photocatalysts. *Chem. Phys. Lett.* **2008**, *457*, 202−205.

(14) Irie, H.; Kamiya, K.; Shibanuma, T.; Miura, S.; Tryk, D. A.; Yokoyama, T.; Hashimoto, K. Visible Light-Sensitive Cu(II)-Grafted TiO_2 Photocatalysts: Activities and X-ray Aabsorption Fine Structure Analyses. *J. Phys. Chem. C* **2009**, *113*, 10761−10766.

(15) Nishikawa, M.; Mitani, Y.; Nosaka, Y. Photocatalytic Reaction Mechanism of Fe(III)-Grafted TiO_2 Studied by Means of ESR Sspectroscopy and Cchemiluminescence Photometry. *J. Phys. Chem. C* **2012**, *116*, 14900−14907.

(16) Nosaka, Y.; Takahashi, S.; Sakamoto, H.; Nosaka, A. Reaction Mechanism of Cu(II)-Grafted Visible-Light Responsive TiO_2 and WO_3 Photocatalysts Studied by Means of ESR Spectroscopy and Chemiluminescence Photometry. *J. Phys. Chem. C* **2011**, *115*, 21283−21290.

(17) Lin, M.; Inde, R.; Nishikawa, M.; Qiu, X.; Atarashi, D.; Sakai, E.; Nosaka, Y.; Hashimoto, K.; Miyauchi, M. Enhanced Photoactivity with Nanocluster-Grafted Titanium Dioxide Photocatalysts. *ACS Nano* **2014**, *8*, 7229−7238.

(18) Geim, A. K.; Novoselov, K. S. The Rise of Graphene. *Nat. Mater.* **2007**, *6*, 183−191.

(19) Bonaccorso, F.; Sun, Z.; Hasan, T.; Ferrari, A. C. Graphene Photonics and Optoelectronics. *Nat. Photonics* **2010**, *4*, 611−622.

(20) Wei, Z.; Wang, D.; Kim, S.; Kim, S.-Y.; Hu, Y.; Yakes, M. K.; Laracuente, A. R.; Dai, Z.; Marder, S. R.; Berger, C.; King, W. P.; de Heer, W. A.; Sheehan, P. E.; Riedo, E. Nanoscale Tunable Reduction of Graphene Oxide for Graphene Electronics. *Science* **2010**, *328*, 1373−1376.

(21) Xiang, Q.; Yu, J.; Jaroniec, M. Graphene-Based Semiconductor Photocatalysts. *Chem. Soc. Rev.* **2012**, *41*, 782−796.

(22) Kamat, P. V. Graphene-Based Nanoassemblies for Energy Conversion. *J. Phys. Chem. Lett.* **2011**, *2*, 242−251.

DOI: 10.1021/am507483q
ACS Appl. Mater. Interfaces 2015, 7, 1816−1823

(23) Krishnamurthy, S.; Kamat, P. V. Galvanic Exchange on Reduced Graphene Oxide: Designing a Multifunctional Two-dimensional Catalyst Assembly. *J. Phys. Chem. C* **2013**, *117*, 571−577.
(24) Xiang, Q.; Yu, J.; Jaroniec, M. Synergetic Effect of MoS_2 and Graphene as Cocatalysts for Enhanced Photocatalytic H_2 Production Activity of TiO_2 Nanoparticles. *J. Am. Chem. Soc.* **2012**, *134*, 6575−6578.
(25) Hummers, W. S.; Offeman, R. E. Preparation of Graphitic Oxide. *J. Am. Chem. Soc.* **1958**, *80*, 1339.
(26) Zhao, K.; Zhang, L.; Wang, J.; Li, Q.; He, W.; Yin, J. J. Surface Structure-Dependent Molecular Oxygen Activation of BiOCl Single-Crystalline Nanosheets. *J. Am. Chem. Soc.* **2013**, *135*, 15750−15753.
(27) Sun, J.; Zhang, H.; Guo, L.-H.; Zhao, L. Two-Dimensional Interface Engineering of a Titania−Graphene Nanosheet Composite for Improved Photocatalytic Activity. *ACS Appl. Mater. Interfaces* **2013**, *5*, 13035−13041.
(28) Xiong, Z.; Zhang, L. L.; Zhao, X. S. Visible-Light-Induced Dye Degradation over Copper-Modified Reduced Graphene Oxide. *Chem.—Eur. J.* **2011**, *17*, 2428−2434.
(29) Yeh, T. F.; Syu, J. M.; Cheng, C.; Chang, T. H.; Teng, H. S. Graphite Oxide as a Photocatalyst for Hydrogen Production from Water. *Adv. Funct. Mater.* **2010**, *20*, 2255−2262.
(30) Perera, S. D.; Mariano, R. G.; Vu, K.; Nour, N.; Seitz, O.; Chabal, Y.; Balkus, K. J. Hydrothermal Synthesis of Graphene-TiO_2 Nanotube Composites with Enhanced Photocatalytic Activity. *ACS Catal.* **2012**, *2*, 949−956.
(31) Rao, R.; Podila, R.; Tsuchikawa, R.; Katoch, J.; Tishler, D.; Rao, A.; Ishigami, M. Effects of Layer Stacking on the Combination Raman Modes in Graphene. *ACS Nano* **2011**, *5*, 1594−1599.
(32) Su, C. Y.; Xu, Y. P.; Zhang, W. J.; Zhao, J. W.; Liu, A. P.; Tang, X. H.; Tsai, C. H.; Huang, Y. Z.; Li, L. J. Highly Efficient Restoration of Graphitic Structure in Graphene Oxide Using Alcohol Vapors. *ACS Nano* **2010**, *4*, 5285−5292.
(33) Reyna-González, J. M.; Torriero, A. A. J.; Siriwardana, A. I.; Burgar, I. M.; Bond, A. M. Extraction of Copper(II) Ions from Aqueous Solutions with a Methimazole-Based Ionic Liquid. *Anal. Chem.* **2010**, *82*, 7691−7698.
(34) Wu, T.; Lin, T.; Zhao, J.; Hidaka, H.; Serpone, N. TiO_2-Assisted Photodegradation of Dyes. 9. Photooxidation of a Squarylium Cyanine Dye in Aqueous Dispersions under Visible Light Irradiation. *Environ. Sci. Technol.* **1999**, *33*, 1379−1387.
(35) Wang, P.; Xia, Y.; Wu, P.; Wang, X.; Yu, H.; Yu, J. Cu(II) as a General Cocatalyst for Improved Visible-Light Photocatalytic Performance of Photosensitive Ag-Based Compounds. *J. Phys. Chem. C* **2014**, *118*, 8891−8898.
(36) Lightcap, I. V.; Kosel, T. H.; Kamat, P. V. Anchoring Semiconductor and Metal Nanoparticles on a Two-Dimensional Catalyst Mat. Storing and Shuttling Electrons with Reduced Graphene Oxide. *Nano Lett.* **2010**, *10*, 577−583.
(37) Kitano, S.; Murakami, N.; Ohno, T.; Mitani, Y.; Nosaka, Y.; Asakura, H.; Teramura, K.; Tanaka, T.; Tada, H.; Hashimoto, K.; Kominami, H. Bifunctionality of Rh^{3+} Modifier on TiO_2 and Working Mechanism of Rh^{3+}/TiO_2 Photocatalyst under Irradiation of Visible Light. *J. Phys. Chem. C* **2013**, *117*, 11008−11016.
(38) Li, X.; Zhen, X.; Meng, S.; Xian, J.; Shao, Y.; Fu, X.; Li, D. Structuring β-Ga_2O_3 Photonic Crystal Photocatalyst for Efficient Degradation of Organic Pollutants. *Environ. Sci. Technol.* **2013**, *47*, 9911−9917.
(39) Zhang, H.; Lv, X.; Li, Y.; Wang, Y.; Li, J. P25-Graphene Composite as a High Performance Photocatalyst. *ACS Nano* **2010**, *4*, 380−386.
(40) Liu, B.; Huang, Y.; Wen, Y.; Du, L.; Zeng, W.; Shi, Y.; Zhang, F.; Zhu, G.; Xu, X.; Wang, Y. Highly Dispersive {001} Facets-Exposed Nanocrystalline TiO_2 on High Quality Graphene as a High Performance Photocatalyst. *J. Mater. Chem.* **2012**, *22*, 7484−7491.
(41) Pan, X.; Zhao, Y.; Liu, S.; Korzeniewski, C. L.; Wang, S.; Fan, Z. Comparing Graphene-TiO_2 Nanowire and Graphene-TiO_2 Nanoparticle Composite Photocatalysts. *ACS Appl. Mater. Interfaces* **2012**, *4*, 3944−3950.

DOI: 10.1021/am507483q
ACS Appl. Mater. Interfaces 2015, 7, 1816−1823